1. INTRODUCTION

Arsenic has been linked to various diseases including skin and bladder cancer (Smith et al. 2002). While some arsenic pollution is associated with anthropogenic inputs, the more widespread and threatening sources are from weathering of arsenic-bearing minerals, such as arsenopyrite (FeAsS), orpiment (As_2S_3), realgar (As_2S_2) and arsenic-rich hydrous ferric oxides (HFOs) (Welch et al. 2001; Nordstrom 2002; Smedley and Kinniburgh 2002; Welch and Stollenwerk 2003) . Elevated levels of arsenic have been found in natural waters in many areas around the world (Nordstrom 2002; Smedley and Kinniburgh 2002). Despite this, little information is available on the oxidation of arsenic-bearing minerals, a process that is a significant source of arsenic to the environment (Smedley and Kinniburgh 2002). Elucidating the rates and mechanisms by which arsenic-bearing minerals weather is an integral step to understanding arsenic retention and release in the environment.

Lengke and Tempel (2002) found that at circumneutral pH and 25°C orpiment (As_2O_3) oxidation by dissolved oxygen (DO) proceeded stoichiometrically with the rate law represented as $r = 10^{11.77}[DO]^{0.36}[H^+]^{-0.47}$ where r represents the rate of arsenic release in mol/m^{2}sec. It was found that arsenic and sulfur were not completely oxidized to sulfate and arsenate over the course of these experiments. This partial oxidation produced arsenite (H_3AsO_3) as the dominant arsenic species, as well as several intermediate sulfur species.

Lengke and Tempel (2003) reported that the corresponding rate law for realgar (AsS) oxidation, measured with respect to arsenic released, may be written as $r = 10^{-9.63}[DO]^{0.51}[H^+]^{-0.28}$ where r represents arsenic released in mol/m^{2}sec. Similar to orpiment, the authors found that oxidation of realgar yielded arsenite as the dominant arsenic species in solution. The results from these two series of experiments help to elucidate the mechanism of oxidation of arsenic sulfides, which bears some similarity to oxidation of other sulfide minerals. Specifically, the reaction order with respect to DO found in Lengke and Tempel's experiments is similar to pyrite oxidation (Williamson and Rimstidt 1994), thus it is possible that orpiment and realgar oxidation shares the same rate-limiting step as pyrite – transfer of electrons to the oxidant.

There have been several reports pertaining to arsenopyrite surface structure and composition during oxidation (Richardson and Vaughan 1989; Foster et al. 1998; Schaufuss et al. 2000). In summary, these studies have shown that arsenic may exist at the unaltered surface as As(0) or As(-I), with subsequent oxidation to As(I), As(III), and As(V) in the presence of air or water. Sulfur, originally present as di-, mono-, and polysulfide, may be released as polysulfides and thiosulfates depending on Eh and pH conditions, but is ultimately converted to sulfate. Iron is present at the surface primarily as Fe(II), and significant accumulation of iron oxyhydroxides is apparent on the surface during oxidation.

There have been only three studies addressing the kinetics of arsenopyrite oxidation (Gagen 1987; Ruitenberg et al. 1999; Yunmei et al. 2004). These studies report dissolution rates for oxidation of arsenopyrite by ferric iron at low pH. However, arsenopyrite weathering does not occur exclusively in acidic environments. At circumneutral pH values, it would be unlikely that Fe^{3+} would be the main oxidant due to its low solubility; oxygen would be the more likely oxidant. Even if, through continual oxidation, the micro-environment near the surface of the arsenopyrite becomes acidic, oxygen will be an important factor in the early oxidation stages before the surface environment becomes acidic.

The objectives of this study are to obtain a laboratory rate and delineate a potential mechanism and rate determining step (RDS) for arsenopyrite oxidation under circumneutral pH conditions with dissolved oxygen as the oxidant. Results of this study are important not only for improving the database of weathering characteristics of arsenic-bearing minerals, but also for predicting release of different forms of arsenic from arsenopyrite weathering in field settings.

2. MATERIALS AND METHODS

2.1 Experimental

In our investigations, the oxidative dissolution rate of arsenopyrite under varying redox conditions and circumneutral pH was determined using an internally stirred mixed flow reactor (MFR) system (Figure 1). Mixed flow reactors are advantageous compared to batch reactors because they measure rates directly, thereby eliminating the need to

differentiate the concentration versus time data produced by batch reactors. More details on the design of the MFR can be found in Weissbart and Rimstidt (2000).

The arsenopyrite used in these experiments was from Mexico and was determined after 56 analyses by electron microscopy to have an average chemical formula of $Fe_{1.02}As_{0.95}S_{1.03}$. The sample was crushed in a mortar and pestle and the 60-80 mesh fraction (177 to 250 micron diameter (Lide 1991)), was retained for use in the experiment. Scanning Electron Microprobe (SEM) analysis of the powder revealed the presence of quartz which was removed by a gravity separation method.

Following sieving, the arsenopyrite was rinsed with 75% ethanol and placed in a sonicator for several minutes to remove ultrafine particles adhering to the surface of the mineral. The supernatant was decanted and the procedure was repeated until the supernatant was clear. The sample was then dried in an oven for approximately an hour at 50-60°C and stored in a dessicator. Nitrogen adsorption BET analysis yielded a surface area of 0.038 m^2/g.

The MFR used in this experiment was machined from a solid acrylic rod. The sample was confined between two nesting o-rings and held in place by 120 nylon mesh attached to the outside of the o-rings with styrene glue. Viton tubing was used for the feed and effluent tubing in order to limit oxygen exchange with the atmosphere.

In each experiment, 1.00 g of arsenopyrite was used. A feed solution of oxygenated 0.01 M NaCl entered the reactor at a rate of 0.325 ± 0.006 mL/min . The reactor was kept immersed, throughout the experiment, in a 25°C water bath. Upon leaving the reactor, the effluent continued through a DO probe reservoir and was collected in 10 mL acid-washed glass test tubes by a fraction collector set to change tubes at 20 minute intervals. Groups of three tubes (representing 1 hour) were preserved in the following pattern: Tube 1 was preserved with HNO_3 for total arsenic, iron, and sulfur analyses, Tube 2 was preserved with EDTA for As speciation, and Tube 3 received no treatment and was used for determining the pH for that hour.

Iron and sulfur concentrations were determined by Inductively Coupled Plasma with Atomic Emission Spectroscopy (ICP-AES). Arsenic concentrations were determined by Graphite Furnace Atomic Absorption Spectroscopy (GFAAS). Detection

limits for iron, sulfur, and arsenic were 3.3, 11.3, and 1.6 µg/L respectively. Arsenic speciation (As^{3+} and As^{5+}) was achieved by strong anion exchange column (SAX) separation, followed by GFAAS analysis to obtain concentrations of each species. SAX separation involves eluting a sample through a column wherein the positively charged and neutral species pass through the column while the negatively charged species are retained on the column and extracted separately with nitric acid (Le et al. 2000; Garbarino et al. 2002).

2.2 Measurements and Calculations

Experiments were run for approximately 24 hours. Varying DO concentrations were established by bubbling the feed solution with different oxygen concentrations (Table 1). Because the feed solution tank and tubing are slightly gas permeable, the actual DO saturation achieved in the feed solution is somewhat lower than would be expected in a closed system. For example, bubbling 60% O_2 gas into the solution yields a maximum DO saturation of 17.1 mg/L, which is lower than the 24.2 mg/L predicted by Henry's law. However, for the purposes of these experiments, it was not necessary to achieve specific DO saturations. Instead, the goal was to maintain a constant value throughout each experiment and to measure rates over a range of DO conditions by performing different trials.

Dissolved oxygen and pH measurements were recorded for the feed solution and effluent using an Orion DO probe (model 081010), Orion pH meter (model 8102BN) and a laptop computer equipped with Orion Sensorlink® software. DO values for the effluent were collected every 10 minutes throughout the experiment. It was found that degassing of the solution did not have a significant effect on pH over a 24 hour period, thus pH values were recorded for each hour at the end of the experiment. Temperature at the level of the sample in the water bath was also monitored and remained at 25 ± 0.2°C.

3. RESULTS

Though sulfur is the more common choice for the reaction progress variable (RPV) for sulfide mineral oxidation due to its conservative behavior, arsenic was chosen as the RPV in this case for the oxidation of arsenopyrite because the method used to

analyze arsenic concentrations, GFAA, is more sensitive than the ICP methods used to measure iron and sulfur concentrations. In addition, pair-wise t-test statistical analyses show that there is no significant difference between the arsenic and sulfur release rates at steady state. While there is some danger in using arsenic as the RPV due to its propensity for adsorbing to iron oxyhydroxides, our data do not show evidence of that behavior. If adsorption were occurring, iron and arsenic data would show similar trends in the steady state release rate versus time data seen in Figure 2. Instead, the arsenic curve closely tracks with the sulfur curve.

Visual interpretation of the graphs of Fe, As, and S concentration versus time for all DO conditions reveals an exponentially decreasing curve as is typical for most mineral dissolution until steady state is reached (example shown in Figure 2). For this investigation, steady state was defined as beginning at the point in time where the change between successive hourly concentration measurements was consistently less than 15%. In all experiments, this occurred for arsenic before 15 hours. Therefore, steady state release rates were calculated for times greater than or equal to 15 hours using the equation (Rosso and Rimstidt 2000):

$$r = \frac{m_i * r_f}{M * A} \qquad (1)$$

r = rate of reaction in mol/m^{2}sec

m_i = molality of i (mol/kg)

r_f = rate of feed solution in kg/sec

M = mass of FeAsS (g)

A = specific surface area of FeAsS (m^2/g).

Linear regression (least squares method) of the steady state release rate data indicate that, within 95% confidence limits, there is a significant difference in iron and sulfur release rates over the tested DO range, while there is no significant difference for arsenic release rates over the same DO range (see Figure 3 caption for regression equations). Pair-wise t-test analysis revealed that the mean iron release rate was significantly different from arsenic and sulfur, though the mean release rates for arsenic and sulfur are statistically the same.

It was expected that arsenopyrite would oxidize according to a rate law of the form

$$r = (Ak)a_{O_2}a_{H^+} \qquad (2)$$

which can be written in logarithmic form as

$$\log r = \log k' + \log a_{O_2} - pH \qquad (3)$$

where k = rate constant (mol/m^{2}sec), a_i = activity of i, and $k' = Ak$ (mol/sec). However, multiple linear regression of the data revealed that the second two terms of equation 3 were not significantly different from zero, indicating that DO concentration and pH have no effect on the oxidation rate of arsenopyrite (see Figure 3 and Table 2). Thus, the oxidation rate for arsenopyrite was calculated as the change in arsenic concentration over time (also equal to change in sulfur concentration) as shown below

$$r = \frac{dn_{Aspy}}{dt} = \frac{dn_{As}}{dt} = \frac{dn_{SO_4}}{dt} \qquad (4)$$

$$r = Ak = A(6.31\times10^{-11}) \qquad (5)$$

where $\frac{dn_i}{dt}$ = molar change in i per time (mol/sec). The rate constant k was calculated as the average of all arsenic steady state release rate data.

The amount of As(V) as a percentage of the total arsenic in solution over time is shown for all DO conditions in Figure 4. Results show that the amount of As(V) found in solution increases over time. Arsenic speciation data can be found in Appendix A.

A summary of the rate data collected for this experiment can be found in Appendix B.

4. DISCUSSION

4.1 Arsenopyrite oxidation rates

If the dissolution of arsenopyrite were congruent, then iron, arsenic and sulfur should be released in a 1:1:1 molar ratio. It can be seen from Figure 3 and from statistical analyses that iron exits the reactor at a rate that is significantly different from arsenic and sulfur, and not according to the correct molar ratio. This may be explained by oxidation of ferrous iron released from the arsenopyrite surface and subsequent

precipitation of iron oxyhydroxides within the MFR system; iron oxyhydroxide formation was observed by Nesbitt and Pratt (1995) in their spectroscopic investigations of the arsenopyrite surface. Analysis of steady state data shows that arsenic and sulfur are released in the correct stoichiometric proportions. The equimolar release of dissolved arsenic and sulfur suggests congruent dissolution of arsenopyrite.

The oxidation rate of arsenopyrite in this study is similar but slower than those reported for some other sulfides (Figure 5). Published literature on the mineralogy of mine tailings suggests that arsenopyrite oxidizes faster than pyrite (see Table 3.4 in (Jambor 1994)), but our laboratory results show that arsenopyrite oxidation is almost an order of magnitude slower than pyrite oxidation.

4.2 Reaction mechanism

The fact that arsenopyrite oxidation rate is not controlled by DO concentration suggests that the mechanism by which arsenopyrite oxidizes is different from that for pyrite (Williamson and Rimstidt 1994) and other arsenic sulfides (Lengke and Tempel 2002; Lengke and Tempel 2003) which show a rate dependence on DO concentrations. While some aspects of the mechanism of oxidation by oxygen for these sulfides may be similar, the results from this study point to a different rate determining step (RDS) for arsenopyrite than for other sulfides. Because the RDS is the slowest step in the overall reaction sequence, it is useful to understand what part of the process is the RDS in order to accurately predict the controls on mineral reaction rates.

To elucidate the mechanism of oxidation for arsenopyrite, it is helpful to visualize the mineral as an electrochemical cell as is described for pyrite by Rimstidt and Vaughan (2003). Using this model, the oxidation of arsenopyrite can be viewed as a series of three concurrent processes consisting of 1) donation of electrons from a cathodic site to the oxidant (O_2 in this case), 2) electron transfer from a anodic site to replace lost electrons at the cathodic site, and 3) generation of electrons at an anodic site by the oxidation of arsenic and sulfur. At anodic sites, water donates oxygen to create AsO_x and SO_x species and releases H^+ to solution to maintain a charge balance with H^+ consumption at the cathodic sites.

Because the arsenopyrite oxidation rate is independent of DO concentrations, we can conclude that the transfer of electrons from arsenopyrite to oxygen at the cathodic site cannot be the rate determining step, as has been found for pyrite (Brown and Jurinak 1989; Rimstidt and Vaughan 2003). Therefore, the oxidation rate must be controlled by either transport of electrons through the solid or addition of oxygen to sulfur and arsenic at the anodic site.

The rate of transport of electrons through the arsenopyrite is controlled by its electrical resistivity. Vaughan and Craig (1978) provide resistivity values for a variety of sulfide minerals. They report that pyrite resistivity ranges from 0.005 to 5 Ohm cm; the one value measured for arsenopyrite is 0.03 Ohm cm. Because pyrite oxidation is limited by the cathodic reaction (i.e., the transfer of electrons from the mineral surface to oxygen) and not electron transport through the solid, and because the arsenopyrite resistivity value is within the range of pyrite values, it appears unlikely, based on these limited data, that electron transport is the rate determining step for arsenopyrite oxidation.

The more likely rate determining step is the addition of oxygen to arsenic and/or sulfur occurring at the anodic site (Figure 6). Arsenic exists on the surface of arsenopyrite most commonly as As^{-1} or As^{0} (Nesbitt and Pratt 1995). Because arsenate is the most thermodynamically stable aqueous form of arsenic under the redox conditions of this experiment, the presence of arsenite in solution, as found in our speciation results (Figure 4), suggests that the kinetics of oxygen attachment to the surface arsenic species is slow, thus allowing arsenite to be released to solution before complete oxidation can occur. Some of the arsenite is subsequently oxidized to arsenate in solution. These results suggest that the attachment of oxygen to the reduced arsenic (and sulfur) species and the subsequent release of AsO_x and SO_x is most likely the slowest, and thus the rate-determining, step in the process of arsenopyrite oxidation.

4.3 Rates in field settings

Observations from this study are useful in determining conditions under which arsenopyrite oxidation will be controlled by ferric iron or oxygen. Such knowledge is integral to understanding the dynamics of arsenic and iron behavior at mine sites where arsenopyrite is prevalent (e.g., Homestake Mine in South Dakota, see Nelson (1974)).

This concept is demonstrated pictorially in Figure 7 where the rate of arsenopyrite oxidation by oxygen is compared to the rate of arsenopyrite oxidation by ferric iron in equilibrium with both ferrihydrite and goethite. This graph was created by assuming 1.0 m^2 of arsenopyrite/ kg of solution; the rate law for arsenopyrite oxidation by iron was taken from Rimstidt et al. (1992), but is also consistent with the results presented in Yunmei et al. (2004). It can be seen from Figure 7 that below a pH of approximately 3, ferric iron controls the oxidation of arsenopyrite, while above pH 3, oxygen is the dominant oxidant because the solubility of ferrihydrite and goethite are low.

Other factors may also influence the ability of iron to dominate the arsenopyrite oxidation process. Primarily, the rate of ferrous iron oxidation in solution could be important in determining the rate and extent of arsenopyrite oxidation by ferric iron. Rates of ferrous iron oxidation vary widely depending on the pH and redox conditions and whether or not there is microbial influence. In general, in a strictly abiotic system, ferrous iron oxidation is slow enough at lower pH to limit the rate of iron oxidation of arsenopyrite, but fast enough nearer to neutral pH to not be rate-limiting (Herbert 1999). In field settings, ferrous iron oxidation rates are microbially-mediated and much faster at lower pH; therefore arsenopyrite oxidation by ferric iron is likely to be fast in field settings.

5. CONCLUSIONS

The rate law for arsenopyrite oxidation by oxygen at circumneutral pH is $r = A(6.76 \times 10^{-11})$ where A = arsenopyrite surface area for DO concentrations between 0.3 and 17.1 mg/L. This rate is comparable to other sulfide minerals such as pyrite, realgar, and orpiment under oxidizing conditions (6.0-7.0 mg/L). Because DO level does not affect the oxidation rate of arsenopyrite, it implies that the mechanism for arsenopyrite oxidation is different from oxidation of other sulfide minerals which are dependent on DO. Results of this study suggest that the rate-determining step for arsenopyrite oxidation likely involves attachment of oxygen at the anodic site instead of electron transfer to the oxidant as in other sulfide minerals.

6. REFERENCES

Brown, A. D. and J. J. Jurinak (1989). "Mechanism of pyrite oxidation in aqueous mixtures." J. of Environ. Qual. **18**: 545-550.

Foster, A. L., G. E. Brown, Jr., et al. (1998). "Quantitative arsenic speciation in mine tailings using X-ray absorption spectroscopy." American Mineralogist **83**: 553-568.

Gagen, P. M. (1987). The oxidation rates of arsenopyrite and chalcopyrite in acidic ferric chloride solutions at 0 to 60 C. Dept. of Geological Sciences. Blacksburg, VA, Virginia Polytechnic Institute and State University.

Garbarino, J. R., A. J. Bednar, et al. (2002). Methods of Analysis by the U.S. Geological Survey National Water Quality Laboratory-Arsenic speciation in natural-water samples using laboratory and field methods. Denver, Colorado, U.S. Geological Survey.

Herbert, R. B. (1999). Sulfide mineral oxidation in mine waste deposits. A review with emphasis on dysoxic weathering. Stockholm, Swedish Foundation for Strategic Environmental Research.

Jambor, J. L. (1994). Mineralogy of sulfide-rich tailings and their oxidation products. Environmental Geochemistry of Sulfide-Mine Wastes. D. W. Blowes, Mineralogical Association of Canada. **22**.

Le, X. C., X. Lu, et al. (2000). "Speciation of submicrogram per liter levels of arsenic in water: On-site species separation integrated with sample collection." Environ. Sci. Technol. **34**(11): 2342-2347.

Lengke, M. F. and R. N. Tempel (2002). "Reaction rates of natural orpiment oxidation at 25 to 40 C and pH 6.8 to 8.2 and comparison with amorphous As_2S_3 oxidation." Geochimica et Cosmochimica Acta **66**(18): 3281-3291.

Lengke, M. F. and R. N. Tempel (2003). "Natural realgar and amorphous AsS oxidation kinetics." Geochimica et Cosmochimica Acta **67**(5): 859-871.

Lide, D. R. (1991). CRC Handbook of Chemistry and Physics. Boston, CRC Press, Inc.

Nelson G. (1974) Gold mineralization at the Homestake gold mine, Lead, South Dakota. *CIM Bulletin* **78**(879), 38.

Nordstrom, D. K. (2002). "Worldwide occurrences of arsenic in ground water." Science **296**: 2143-2145.

Richardson, S. and D. J. Vaughan (1989). "Arsenopyrite: a spectroscopic investigation of altered surfaces." Mineralogical Magazine **53**: 223-229.

Rimstidt J. D., Chermak J. A., and Gagen P. M. (1992) Environmental geochemistry of sulfide oxidation. *204th National Meeting of the American Chemical Society*, 2-13.

Rimstidt, J. D. and D. J. Vaughan (2003). "Pyrite oxidation: A state-of-the-art assessment of the reaction mechanism." Geochimica et Cosmochimica Acta **67**.

Rosso, J. J. and J. D. Rimstidt (2000). "A high resolution study of forsterite dissolution rates." Geochimica et Cosmochimica Acta **64**(5): 797-811.

Ruitenberg, R., G. S. Hansford, et al. (1999). "The ferric leaching kinetics of arsenopyrite." Hydrometallurgy **52**: 37-53.

Schaufuss, A. G., H. W. Nesbitt, et al. (2000). "Reactivity of surface sites on fractures arsenopyrite (FeAsS) toward oxygen." American Mineralogist **85**(11-12): 1754-1766.

Smedley, P. L. and D. G. Kinniburgh (2002). "A review of the source, behavior and distribution of arsenic in natural water." Applied Geochemistry **17**: 517-568.

Smith, A. H., P. A. Lopipero, et al. (2002). "Arsenic epidemiology and drinking water standards." Science **296**: 2145-2146.

Vaughan D. J. and Craig J. R. (1978) Mineral Chemistry of Metal Sulfides, pp. 102. Cambridge University Press.

Weissbart E. J. and Rimstidt J. D. (2000) Wollastonite: Incongruent disslolution and leached layer formation. *Geochimica et Cosmochimica Acta* **64**(23), 4007-4016.

Welch, A. H. and K. G. Stollenwerk (2003). Arsenic in Groundwater, Kluwer Academic Publishers.

Welch, A. H., D. B. Westjohn, et al. (2001). "Arsenic in Ground Water of the United States: Occurrence and Geochemistry." Ground Water **38**(4): 589-604.

Williamson, M. A. and J. D. Rimstidt (1994). "The kinetics and electrochemical rate-determining step of aqueous pyrite oxidation." Geochimica et Cosmochimica Acta **58**(24): 5443-5454.

Yunmei, Y., Z. Yongxuan, et al. (2004). "A kinetic study of the oxidation of arsenopyrite in acidic solutions: implications for the environment." Applied Geochemistry **19**(3): 435-444.

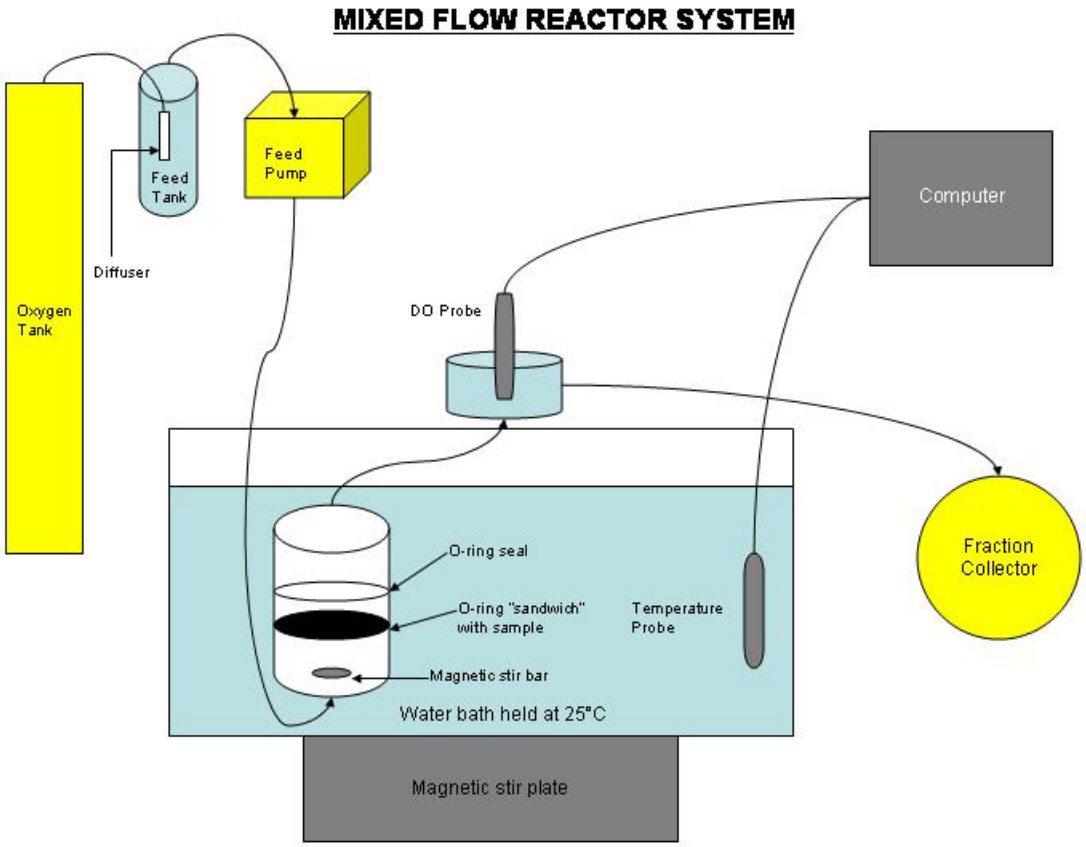

Fig.1. Schematic of the internally stirred mixed flow reactor system. Oxygenated feed solution enters a port at the bottom of the reactor where the solution is mixed by a magnetic stir bar. Solution flows over the fixed bed of arsenopyrite, and out the port at the top of the reactor. The DO of the solution is measured and recorded before collection in the autosampler.

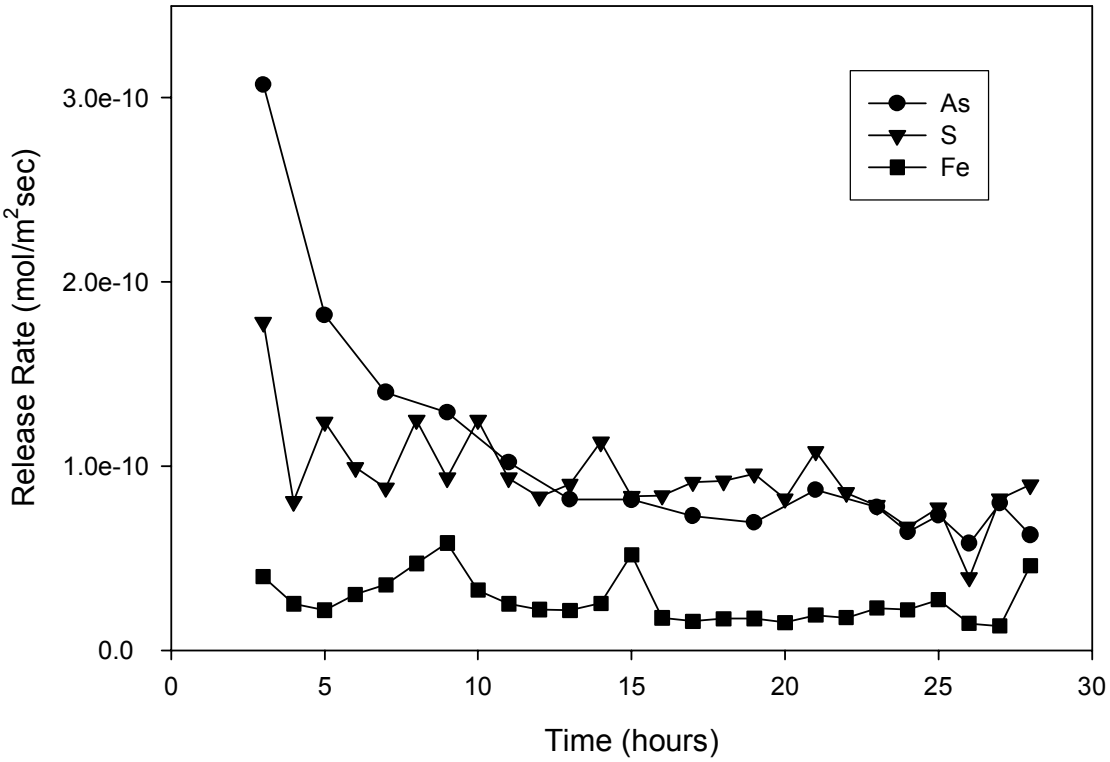

Fig. 2. Release rates versus time for As, S, and Fe under DO = 0.4 mg/L. Data for the first two hours are not plotted because they are out of range on the graph, but are included in the appendix. Release rates for all elements are much higher in the initial phase of the experiment as the rough surface of the mineral is highly reactive. Rates decrease and stabilize as steady state is approached at approximately 15 hours.

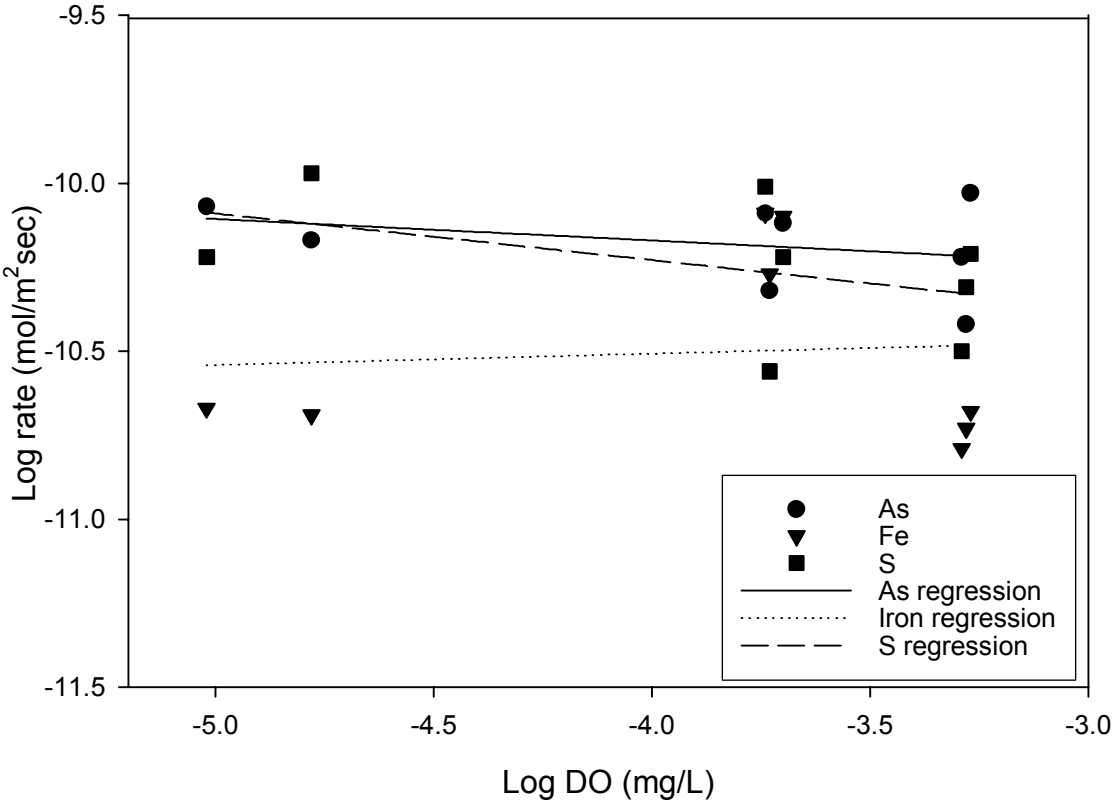

Fig. 3. Log steady state release rate versus log dissolved oxygen for dissolved As, S, and Fe over the tested DO range. Statistical analysis shows that there is no significant dependence of As release rates on DO, while there is a significant (but slight) dependence of Fe and S release rates on DO. Regression equations, with p values are listed below.

$$\log r_{As} = -0.0188(\pm 0.0268, P = 0.49)\log DO + 0.0497(\pm 0.0217, P = 0.03)\, pH - 10.58(\pm 0.141, P = 0.00)$$

$$\log r_{Fe} = -0.084(\pm 0.044, P = 0.060)\log DO - 0.279(\pm 0.036, P = 0.00)\, pH - 8.99(\pm 0.23, P = 0.00)$$

$$\log r_{S} = -0.112(\pm 0.035, P = 0.002)\log DO + 0.036(\pm 0.032, P = 0.26)\, pH - 10.93(\pm 0.21, P = 0.00)$$

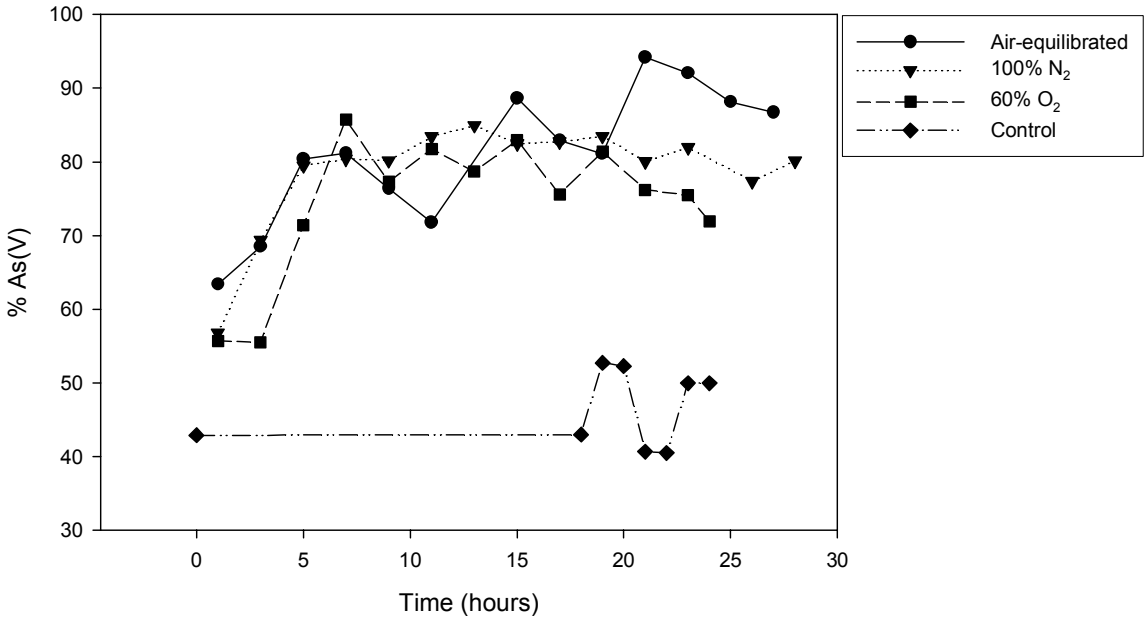

Fig.4. Amount of As(V) as a percentage of the total arsenic in solution over time for the tested DO range. The control experiment was conducted by pumping 100 µg/L As(III) through the MFR system without arsenopyrite under air-equilibrated conditions. The resultant DO concentrations for the air-equilibrated, 100% N_2, and 60% O_2 experiments were 6.1, 0.4, and 16.9 mg/L, respectively.

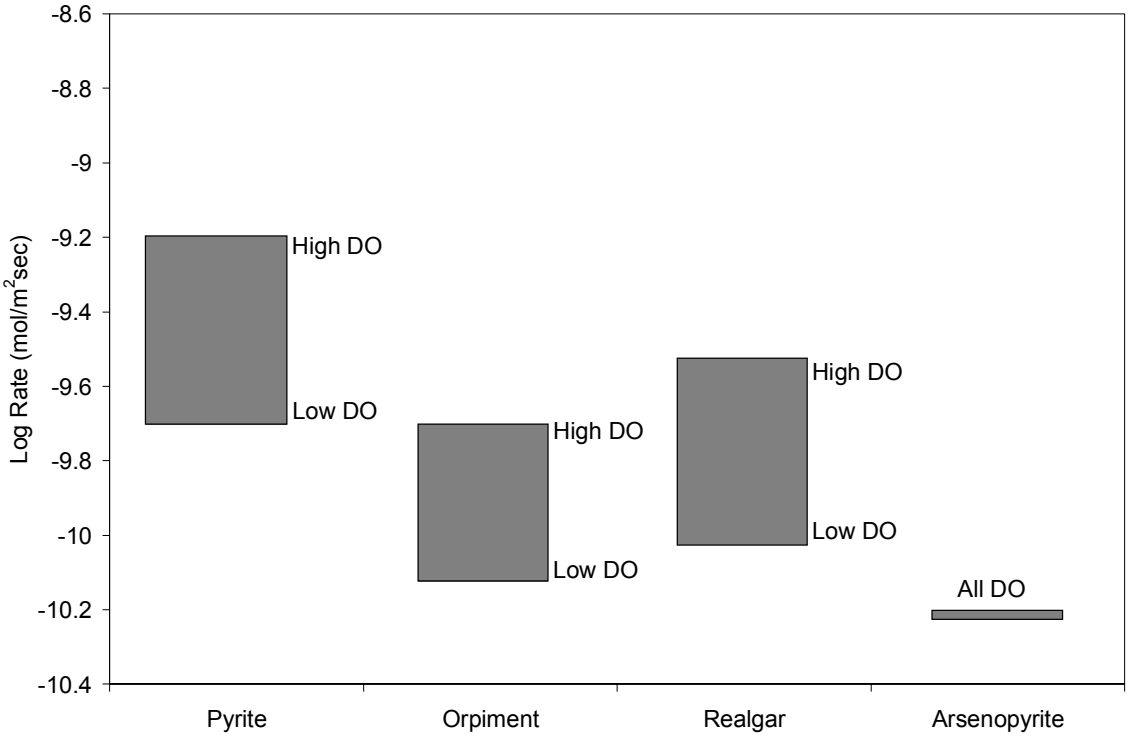

Fig. 5. Oxidation rates for pyrite (Williamson and Rimstidt 1994), orpiment (Lengke and Tempel 2002), realgar (Lengke and Tempel 2003), and arsenopyrite (current study) at high DO (9 mg/L) and low DO (0.9 mg/L).

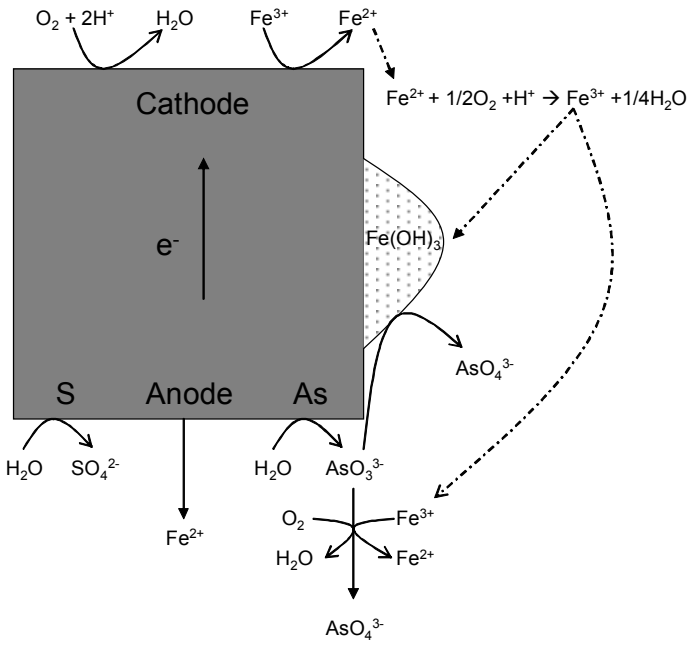

Fig.6. Schematic illustration of the reactions occurring at or near the arsenopyrite surface.

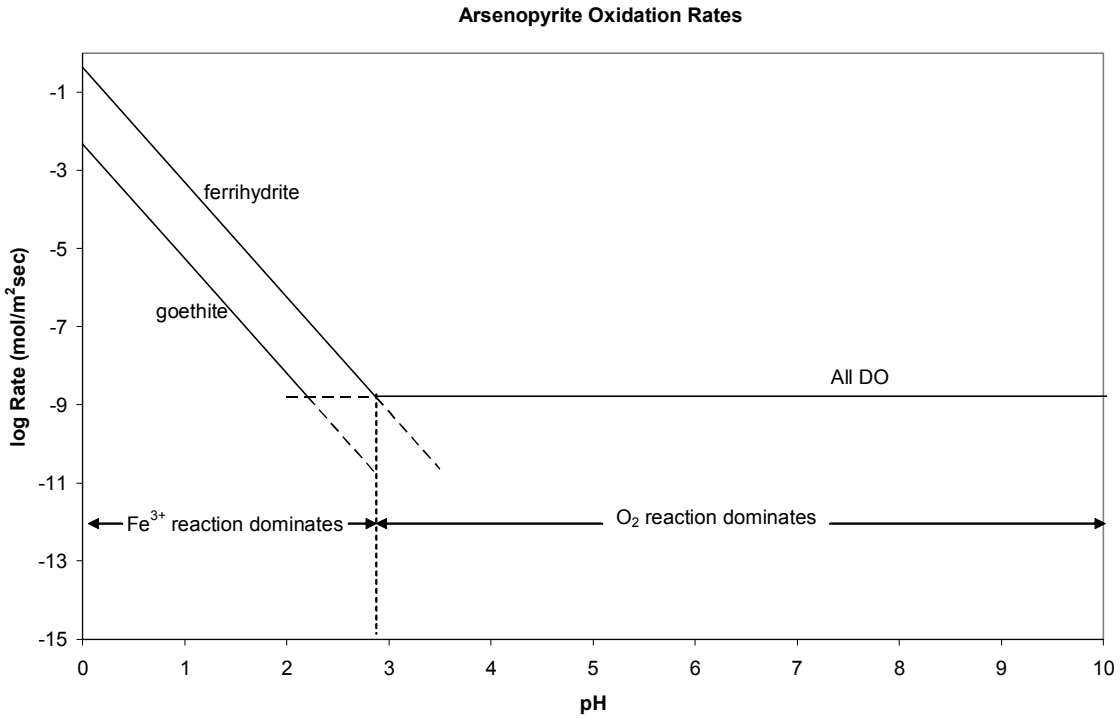

Fig. 7. Comparison of arsenopyrite oxidation rates by oxygen and by Fe(III) in equilibrium with ferrihydrite and goethite assuming 1.0 m^2 arsenopyrite/kg solution. Rate law for arsenopyrite oxidation by iron was taken from Rimstidt et al. (1992).

Table 1. Experimental conditions

Experiment	Gas Feed	Initial DO (mg/L)	Initial (feed) pH
ASP082403	60% O_2, 30% N_2	16.5	6.4
ASP090703	60% O_2, 30% N_2	16.5	6.8
ASP091403	60% O_2, 30% N_2	17.1	7.7
ASP090303	air-equilibrated	6.0	5.7
ASP091203	air-equilibrated	6.3	5.8
ASP090903	100% N_2	0.5	7.6
ASP091003	100% N_2	0.3	7.5

Table 2. Average steady state rate and corresponding initial pH and DO values for each experiment

Experiment	pH	DO (mg/L)	Rate (mol/m^2sec)	n
ASP082403	6.4	16.5	3.83×10^{-11}	5
ASP090703	6.8	16.5	5.95×10^{-11}	6
ASP091403	7.7	17.1	9.35×10^{-11}	7
ASP090303	5.7	6.0	4.85×10^{-11}	6
ASP091203	5.8	6.3	8.15×10^{-11}	10
ASP090903	7.6	0.5	6.73×10^{-11}	10
ASP091003	7.5	0.3	8.49×10^{-11}	7

Overall Average Rate: $6.76 \times 10^{-11} \pm 30\%$

APPENDIX A - Arsenic Speciation Data

ASP082403

Time (hours)	Total As	As(III)	As(V)
1	144.639	73.7268	52.743
3	30.3231	17.2586	21.7217
5	18.4178	10.6363	9.9059
7	28.9284	13.6067	18.3102
9	25.0467	12.5839	21.244
11	23.6415	10.6141	16.7915
13	21.4071	8.3053	15.6838
15	20.6202	7.7224	14.3763
17	20.8124	7.3749	13.0466
19	19.5256	6.7457	15.6511
21	21.1629	7.7558	14.8497
24	20.4718	7.4773	16.5236

ASP090303

Time (hours)	Total As	As(III)	As(V)
1	947.128	325.329	360.66
3	235.387	75.0568	83.3037
5	120.331	39.9959	49.1768
7		32.5855	42.1666
9	69.8791	39.9568	30.591
11	57.6694	20.1859	27.1451
13	56.6481	25.1959	30.0237
15	63.8184	27.2924	29.8914
17	53.7168	19.9192	24.9185
19	48.2501	21.2581	23.6493
21	42.7845	20.7379	22.1238
23	38.9126	17.9089	19.3045

ASP090903

Time (hours)	Total As	As(III)	As(V)
1		255.85	336.28
3	184.71	46.35	105.02
5	109.77	18.99	73.63
7	92.4	15.69	64.32
9	85.42	13.34	53.93
11	62.51	8.64	43.48
13	47.77	6.74	37.94
15	46.29	7.44	34.98
17	38.17	5.75	27.54
19	36.46	5.82	29.36
21	39.05	7.29	29.23
23	35.18	5.88	26.7
24	34.32		
25	32.51		
26	31.12	6.75	23.04
27	34.07		
28	33.55	6.26	25.24

ASP091403

Time (hours)	Total As	As(III)	As(V)
1	401.46	221.4	278.60
3	131.617	104.8	130.90
5	79.5623	48.35	120.9
7	92.6971	30.35	182.5
9	52.9641	21.40	72.80
11	49.1659	19.95	89.10
13	47.1814	18.75	69.15
15	47.9799	12.95	62.90
17	46.7971	19.95	61.70
19	48.4709	13.10	57.30
21	48.5452	15.15	48.55
23	52.8965	13.60	41.80
25	51.9275	12.25	31.40
27	59.7696	15.55	27.00

ASP091203

Time (hours)	Total As	As(III)	As(V)
1	537.716	140.07	242.726
3	286.244	40.3765	87.903
5	180.06	16.0313	65.7063
7	137.788	19.8657	85.7176
9	111.83	24.8191	80.323
11	86.0917	17.8092	45.2756
13	79.2027	130.562	48.5452
15	62.6703	6.495	50.6313
17	52.7505	9.6411	46.853
19	45.9841	10.7548	46.1886
21	39.1877	8.3262	135.678
23	34.72	6.5761	76.3157
24	39.5462		
25	34.4088	6.5044	48.4083
26	26.9655		
27	30.5661	7.652	49.9033

APPENDIX B - Release Rate Data

	Iron Release Rates							
	100% N_2		*Air saturated*			*60% O_2*		
Time elapsed (hr)	**ASP090903**	**ASP091003**	**ASP082803**	**ASP090303**	**ASP091203**	**ASP082403**	**ASP090703**	**ASP091403**
1	4.50E-10	6.02E-10	7.19E-10	9.79E-10	8.77E-10	1.76E-10	1.44E-10	4.16E-10
2	2.14E-10	6.89E-11	1.04E-09	6.12E-10	8.43E-10	2.80E-11	1.86E-09	5.68E-11
3	6.13E-11	1.84E-11	6.44E-10	2.41E-10	6.11E-10	1.14E-10	1.10E-09	2.14E-11
4	3.53E-11	1.51E-11	1.03E-10	2.12E-10	3.32E-10	9.25E-12	3.91E-10	2.21E-11
5	2.68E-11	1.67E-11	3.19E-11	1.24E-10	2.49E-10	1.43E-11	8.27E-11	2.21E-11
6	4.73E-11	1.34E-11	1.91E-11	1.14E-10	2.36E-10	9.25E-12	6.31E-11	2.80E-11
7	4.20E-11	2.90E-11	2.24E-11	2.15E-08	2.23E-10	1.00E-11	1.84E-11	2.19E-11
8	5.40E-11	4.01E-11	1.49E-11	8.76E-11	2.24E-10	2.80E-11	1.66E-11	3.74E-11
9	5.88E-11	5.76E-11	2.06E-11	8.91E-11	1.75E-10	2.33E-11	1.99E-11	3.05E-11
10	4.95E-11	1.57E-11	2.70E-11	6.97E-11	1.70E-10	2.00E-11	1.86E-11	2.24E-11
11	3.63E-11	1.41E-11	1.96E-11	3.39E-10	1.44E-10	1.83E-11	7.30E-11	1.48E-11
12	3.13E-11	1.29E-11	1.67E-11	5.12E-11	1.31E-10	2.33E-11	2.09E-11	4.28E-11
13	2.05E-11	2.27E-11	6.54E-11	9.35E-11	1.20E-10	2.18E-11	2.90E-11	1.92E-11
14	2.38E-11	2.73E-11	3.12E-11	1.52E-10	1.13E-10	3.65E-11	2.01E-11	8.34E-11
15	2.55E-11	7.83E-11	2.16E-11	1.09E-10	1.32E-10	2.05E-11	1.99E-11	8.51E-11
16	2.18E-11	1.34E-11	4.22E-11	8.45E-11	1.11E-10	1.83E-11	2.43E-11	2.16E-11
17	1.38E-11	1.77E-11	1.34E-10	8.12E-11	1.19E-10	1.28E-11	1.64E-11	1.30E-11
18	2.13E-11	1.29E-11	1.88E-11	8.43E-11	7.88E-11	1.80E-11	1.66E-11	1.48E-11
19	1.80E-11	1.64E-11	2.03E-11	8.22E-11	6.92E-11	1.53E-11	1.59E-11	1.16E-11
20	2.13E-11	8.83E-12	2.19E-11	8.27E-11	7.07E-11	1.78E-11	1.37E-11	1.40E-11
21	1.75E-11	2.07E-11	1.70E-11	9.25E-11	7.29E-11	2.25E-11	1.96E-11	3.37E-11
22	1.93E-11	1.62E-11	2.73E-11	6.63E-11	6.04E-11	2.55E-11	1.07E-11	2.78E-11
23	3.20E-11	1.39E-11	2.01E-11	6.63E-11	5.53E-11	1.88E-11	1.09E-11	1.72E-11
24	2.18E-11	2.22E-11	3.37E-10	5.89E-11	7.22E-11	1.93E-11	1.76E-11	1.72E-11
25	2.28E-11	3.21E-11			5.26E-11			2.04E-11
26		1.46E-11			6.48E-11			1.48E-11
27	1.15E-11	1.49E-11			9.81E-11			1.87E-11
28	2.35E-11	6.82E-11			7.39E-11			1.45E-11

	Sulfur Release Rates							
	100% N_2		*Air saturated*			*60% O_2*		
Time elapsed (hr)	**ASP090903**	**ASP091003**	**ASP082803**	**ASP090303**	**ASP091203**	**ASP082403**	**ASP090703**	**ASP091403**
1	3.67E-09	2.64E-09	1.93E-09	2.85E-09	2.50E-09	2.57E-09	3.47E-09	2.38E-09
2	5.49E-10	4.94E-10	7.54E-10	7.14E-10	6.50E-10	4.35E-10	8.72E-10	4.90E-10
3	1.76E-10	1.79E-10	4.94E-10	2.73E-10	5.38E-10	1.24E-10	3.83E-10	1.66E-10
4	3.93E-11	1.22E-10	2.00E-10	4.33E-10	1.43E-10	1.67E-10	2.06E-10	1.22E-10
5	1.16E-10	1.31E-10	1.18E-10	2.32E-10	1.17E-10	6.69E-11	2.72E-10	9.42E-11
6		9.91E-11	8.39E-11	8.40E-11	1.29E-10	3.61E-11	2.20E-10	9.14E-11
7		8.81E-11	6.26E-11	8.12E-09	1.08E-10	4.19E-11	8.35E-11	8.33E-11
8	1.62E-10	8.93E-11	5.23E-11	5.75E-11	1.01E-10	6.14E-11	1.76E-10	6.60E-11
9	9.15E-11	9.57E-11	4.37E-11	1.93E-10	8.84E-11	1.08E-10	7.68E-11	6.73E-11
10	1.62E-10	8.68E-11	1.91E-10		7.70E-11	4.77E-11	1.24E-10	5.70E-11
11	1.07E-10	8.00E-11	3.60E-11	3.47E-11	5.82E-10	1.70E-11	6.25E-11	5.82E-11
12	8.92E-11	7.74E-11	3.09E-11		4.12E-10	4.28E-11	1.85E-10	5.68E-11
13	9.44E-11	8.58E-11		2.62E-11	2.54E-10		1.12E-10	5.28E-11
14	1.48E-10	7.84E-11	4.27E-11	1.18E-10	7.61E-11	4.19E-11	1.61E-10	4.75E-11
15	9.18E-11	7.55E-11	1.87E-11	0.00E+00	7.13E-11		4.85E-11	6.17E-11
16	1.02E-10	6.58E-11	2.79E-11	0.00E+00	8.61E-11	1.49E-10	7.83E-11	5.25E-11
17	9.49E-11	8.77E-11			7.74E-11	9.33E-11	3.52E-11	4.66E-11
18	9.89E-11	8.47E-11			6.64E-11	4.41E-11	1.91E-11	4.91E-11
19	1.19E-10	7.28E-11		1.44E-10	5.51E-11	1.70E-11	1.83E-11	7.01E-11
20	9.65E-11	6.81E-11			5.51E-11	2.79E-11	1.85E-11	5.81E-11
21	1.75E-10	4.01E-11		5.35E-11	5.71E-11	5.92E-11		6.84E-11
22	1.19E-10	5.23E-11		1.32E-10	4.23E-11	5.05E-11	2.64E-11	6.75E-11
23	1.10E-10	4.73E-11			4.99E-11	6.33E-11	3.13E-11	7.41E-11
24	8.38E-11	5.01E-11	2.88E-11		6.90E-11	2.84E-11	2.15E-11	6.22E-11
25	9.37E-11	6.08E-11			5.04E-11			6.48E-11
26	8.99E-11	3.95E-11			4.88E-11			6.14E-11
27	1.13E-10	5.14E-11			5.59E-11			6.01E-11
28	1.20E-10	5.99E-11			6.73E-11			5.42E-11

			Arsenic Release Rates					
	100% N_2		*Air saturated*			*60% O_2*		
Time elapsed (hr)	**ASP090903**	**ASP091003**	**ASP082803**	**ASP090303**	**ASP091203**	**ASP082403**	**ASP090703**	**ASP091403**
1		1.06E-09	1.24E-09	1.81E-09	9.80E-10	2.70E-10	1.82E-09	7.35E-10
3	3.44E-10	2.70E-10	6.30E-10	4.49E-10	5.22E-10	5.65E-11	1.29E-09	2.42E-10
5	2.05E-10	1.60E-10	1.38E-10	2.30E-10	3.28E-10	3.43E-11	2.46E-10	1.46E-10
7	1.72E-10	1.07E-10	9.77E-11		2.51E-10	5.39E-11	1.42E-10	1.71E-10
9	1.59E-10	9.80E-11	7.66E-11	1.10E-10	2.04E-10	4.66E-11	1.17E-10	9.72E-11
11	1.17E-10	8.84E-11	6.87E-11	1.08E-10	1.57E-10	4.40E-11	9.90E-11	8.98E-11
13	8.91E-11	7.45E-11	6.39E-11	1.22E-10	1.44E-10	3.99E-11	8.29E-11	8.62E-11
15	8.63E-11	7.72E-11	5.39E-11	1.03E-10	1.14E-10	3.84E-11	7.37E-11	8.80E-11
17	7.12E-11	7.45E-11	5.30E-11	9.22E-11	9.63E-11	3.88E-11	6.57E-11	8.62E-11
19	6.81E-11	7.06E-11	4.70E-11	8.17E-11	8.39E-11	3.64E-11	6.37E-11	8.80E-11
21	7.29E-11	1.01E-10	4.49E-11	7.43E-11	7.15E-11	3.95E-11	5.52E-11	8.98E-11
23	6.56E-11	8.96E-11	4.34E-11	6.91E-11	6.33E-11	3.82E-11	4.92E-11	9.72E-11
24	6.40E-11			6.91E-11	7.20E-11		4.98E-11	
25	6.06E-11	8.56E-11			6.27E-11			9.53E-11
26	5.80E-11				4.92E-11			
27	6.36E-11	9.60E-11			5.58E-11			1.10E-10
28	6.26E-11				5.25E-11			